Int J Adv Manuf Technol (2018) 94:227–237
DOI 10.1007/s00170-017-0906-9

ORIGINAL ARTICLE

A pyramid-shaped machining test to identify rotary axis error motions on five-axis machine tools: software development and a case study

Soichi Ibaraki[1] · Shota Tsujimoto[2] · Yu Nagai[2] · Yasutaka Sakai[3] · Shigeki Morimoto[3] · Yosuke Miyazaki[3]

Received: 6 May 2017 / Accepted: 31 July 2017 / Published online: 9 August 2017

Abstract The pyramid-shaped machining test was proposed to evaluate error motions of a five-axis machine tool. This paper presents software to perform and analyze the pyramid-shaped machining test. The paper presents an extension of the analysis algorithm to a five-axis machine tool with two rotary axes on the tool side. An experimental case study shows that position and orientation errors (location errors) of rotary axis average lines, as well as position-dependent error motions of a rotary axis, can be numerically identified from geometric errors of the finished test piece. Experimental demonstration of the numerical compensation of rotary axis geometric errors based on the R-test is also presented, along with its performance investigation by the present machining test. The developed software is commercially available.

Keywords Five-axis machine tool · Machining test · Metrology · Error calibration · Geometric error

✉ Soichi Ibaraki
ibaraki@hiroshima-u.ac.jp

1 Department of Mechanical Systems Engineering, Hiroshima University, Kagamiyama 1-4-1, Higashi Hiroshima, Hiroshima 739-8527, Japan

2 Department of Micro Engineering, Kyoto University, Katsura, Nishigyo-ku, Kyoto 615-8530, Japan

3 Fukuda Corporation, 11-2, Akashi-cho, Chuo-ku, Tokyo 104-0044, Japan

1 Introduction

Machine tools with two rotary axes to tilt a tool and/or a workpiece, in addition to three orthogonal linear axes, are collectively called five-axis machine tools. In ISO 230-1 [1], geometric errors of linear and rotary axes are categorized as follows: (a) position and orientation errors of linear or rotary axis average line (called location errors in ISO 230-7 [2]), often caused by the assembly error of machine components, (b) static or quasi-static error motions of linear or rotary axis, parameterized as position-dependent 6-DOF (degrees of freedom) position and orientation errors, and (c) dynamic and transient errors. For machine tool builders, their calibration is a key to ensure the required accuracy over the entire workspace. Numerous error calibration schemes for five-axis machines can be found in the literature, and their good review is in [3, 4]. For example, ISO/TC39/SC2 has lately revised ISO 10791-1 [5] with static tests focusing on (a) and (b), and ISO 10791-6 [6] with dynamic interpolation tests focusing on (a) to (c).

Although it is important to evaluate rotary axis geometric errors by such a non-cutting test, typical machine tool users consider more the machine's accuracy when it performs actual machining. Non-cutting tests are sometimes performed when the machine is "cold" without sufficient machine warm-up. In normal operating conditions with spindle rotation, the machine's geometric errors may be significantly different. For this reason, a machining test is often considered crucial to evaluate a machine's actual performance.

This paper presents a machining test to evaluate quasi-static error motions of a five-axis machine tool. According to ISO 230-1 [1] (Annex B), machining tests related to a machine tool's quasi-static geometric accuracy should be performed as the machine tool moves slowly and behaves in a quasi-static manner, i.e., with no dynamic influences and servo control limitations. The machine tool should not be influenced by any significant machining forces, which is the case for most finishing cuts. In our view, such machining tests proposed for five-axis machines in the literature can be categorized as follows:

The tests requiring simultaneous five-axis synchronization. The test piece's surfaces are finished with synchronously operating five axes. Typical ones are the cone frustum test described in M3 test of ISO 10791-7 [7] (originally in NAS979 [8]; many researchers presented its analysis [9, 10]), and the S-curve test [11, 12], proposed as an amendment to ISO 10791-7 [13] (currently under discussion at ISO TC39/SC2). All error motions of each axis are superimposed onto the finished test piece's geometric error. They can be a good acceptance test for machine tool manufacturers/users to evaluate the machine's overall accuracy, but it would be difficult, or not possible, to use it for a diagnosis test to separately identify each error cause. The NCG recommendation 2005 ("http://www.ncg.de"), the truncated square pyramid test [14], the cubic box test finished by ball end milling at different angular positions [15], the ball end milling test of hemisphere [16], can be seen as this type of tests.

The tests designed to observe single error cause. The tests are designed such that a single error motion of a linear or rotary axis is copied as the finished test piece's geometric error. The tests M1 and M2 in ISO 10791-7 [7] are designed to separately observe each error motion of linear axes, e.g., the squareness error, the straightness error motion, or the linear positioning error motion. Simpler cutting tests, e.g., a planar grinding test [17], a grooving test by a single-point cutting tool [18], and a grooving test with two rotary axis operations [19], can be used to calibrate the position of rotary axis average lines. These tests can be seen as a "direct" test (the term by Schwenke et al. [3]) for linear or rotary axis error motions.

The tests to indirectly identify multiple error causes. According to Schwenke et al. [3], "indirect" tests measure the tool center point (TCP) location as the superposition of multiple error causes and separately identify each error motion using numerical fitting to the machine's kinematic model. In [20], a part of the authors proposed the pyramid-shaped machining test such that all position and orientation errors of rotary axis average lines can be separately identified by evaluating the finished test piece's geometric error. The test M4 in ISO 10791-7 [7] can be seen as a sub-set of the test in [20]. Velenosi et al. [21] presented an analogous test.

It must be emphasized that the tests above evaluate the geometric accuracy of the finished test piece, not its surface finish. The tool geometry, error motions of spindle, the dynamic cutting force, the dynamic displacement (vibration) of a machine, a tool, or a workpiece may influence the roughness profile of the finished surface. Numerous studies have discussed such influence in end milling processes; only recent works include [22–26]. The influence on the surface finish is not in this paper's scope.

For the tests to indirectly identify multiple error causes, error diagnosis requires numerical best fitting of the finished test piece's geometry to the machine's kinematic model. It would be quite beneficial for test users to develop software to perform this calculation. For practical, industrial implementation of the pyramid-shaped machining test proposed in [20], we developed software to perform and analyze this test. The software is now commercially available from Fukuda Corp ("http://www.fukudaco.co.jp/"). This paper's original contributions are as follows:

- This paper presents the software implementation of the analysis algorithm to visually display the finished test piece's geometric error and, then, to identify rotary axis error motions from it. Minor modifications are made on the algorithm presented in [20].
- Reference [20] only presented an analysis algorithm for a five-axis machine tool with two rotary axes on the workpiece side. This paper formulates its extension to a five-axis machine with two rotary axes in the spindle side.
- Experimental demonstration is presented to illustrate the functionalities of the software.
- Additionally, experimental demonstration of the numerical compensation of rotary axis geometric errors is

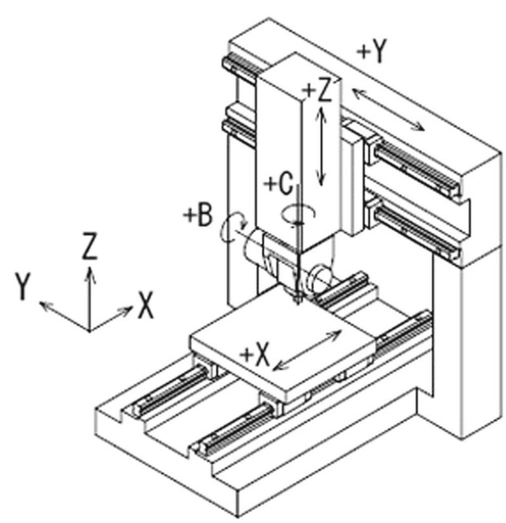

Fig. 1 Machine configuration

presented. The numerical compensation is designed based on the R-test, and its performance is investigated by the present machining test.

2 Pyramid-shaped machining test

This section briefly reviews the machining test proposed in [20]. While [20] targets a five-axis machine with two rotary axes in the workpiece side, this paper considers the machine configuration shown in Fig. 1. The rotating head (C-axis) and the tilting head (B-axis) will be tested. The structural code, according to [5], is [w X' b Y Z C B (C1) t].

Figure 2 depicts the machining test procedure. (a) A square step is end-milled at $B = C = 0°$ by driving X- and Y-axes only. This step is hereafter called the reference step. (b) It is repeated at $C = 90, 180, 270°$ to make total four steps. (c) A square step is machined at the side face at $B = C = 90°$. It is repeated at $C = 0, 180, 270°$ on each side face. (d) It is repeated at $B = -90°$ and $C = 0, 90, 180, 270°$ to make the second step on each side face.

Figure 3 shows the finished test piece's nominal geometry. The dimensions, L and H, should be designed depending on, e.g., the machine size. Then, the finished test piece's geometry is measured preferably by using a coordinate measuring machine (CMM). Figure 4 shows example measured points. The measurement coordinate system is set up based on the position and the orientation of the topmost reference step. (1) Its X-axis is aligned to the -Y side face of the reference step, (2) its Y-axis is parallel to one of the bottom faces of the reference step, and (3) the (X,Y) position of its origin is at the center of the reference step, and its Z position is on the average plane of four bottom faces of the reference step. The measurement coordinate system is also shown in Fig. 3. The geometric tolerance symbols and surface names (S_{**}) in Fig. 3 will be referred in Section 5.3.

3 Overview of software

The major features of the developed software are as follows:

(i) *Generation of NC program*: an NC program to finish the test piece is generated.
(ii) *Graphical presentation of the finished test piece's geometry*: the CMM measurement data are imported and the 3D geometry of the finished test piece is graphically shown. See Section 5.2.
(iii) *Numerical identification of rotary axis error motions*: from the finished test piece's geometry, error motions (position-dependent geometric errors) of rotary axes, as well as position and orientation errors of rotary axis average lines (location errors), are numerically identified. See Section 4.

4 Algorithm to identify rotary axis error motions from the finished test piece's geometry

4.1 Kinematic model and geometric error parameters

"Indirect" calibration schemes reviewed in [3, 4] are based on the kinematic model of five-axis configuration. Although

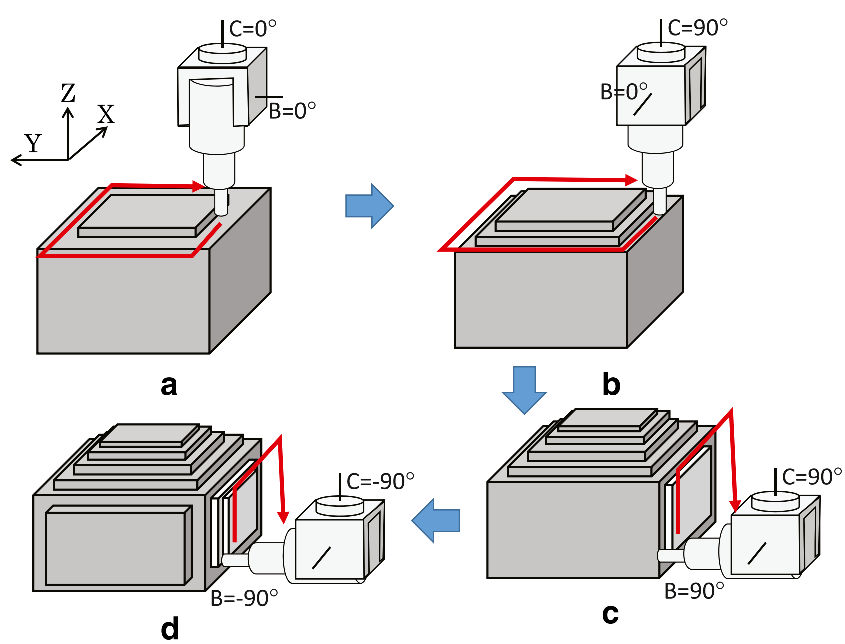

Fig. 2 Machining test procedure. **a** A square step is machined at $B = C = 0°$. **b** It is repeated at $C = 90, 180, 270°$ to make total four steps. **c** A square step is machined at the side face at $B = C = 90°$. It is repeated at $C = 0, 180, 270°$ on each side face. d) It is repeated at $B = -90°$ and $C = 0, 90, 180, 270°$ to make the second step on each side face

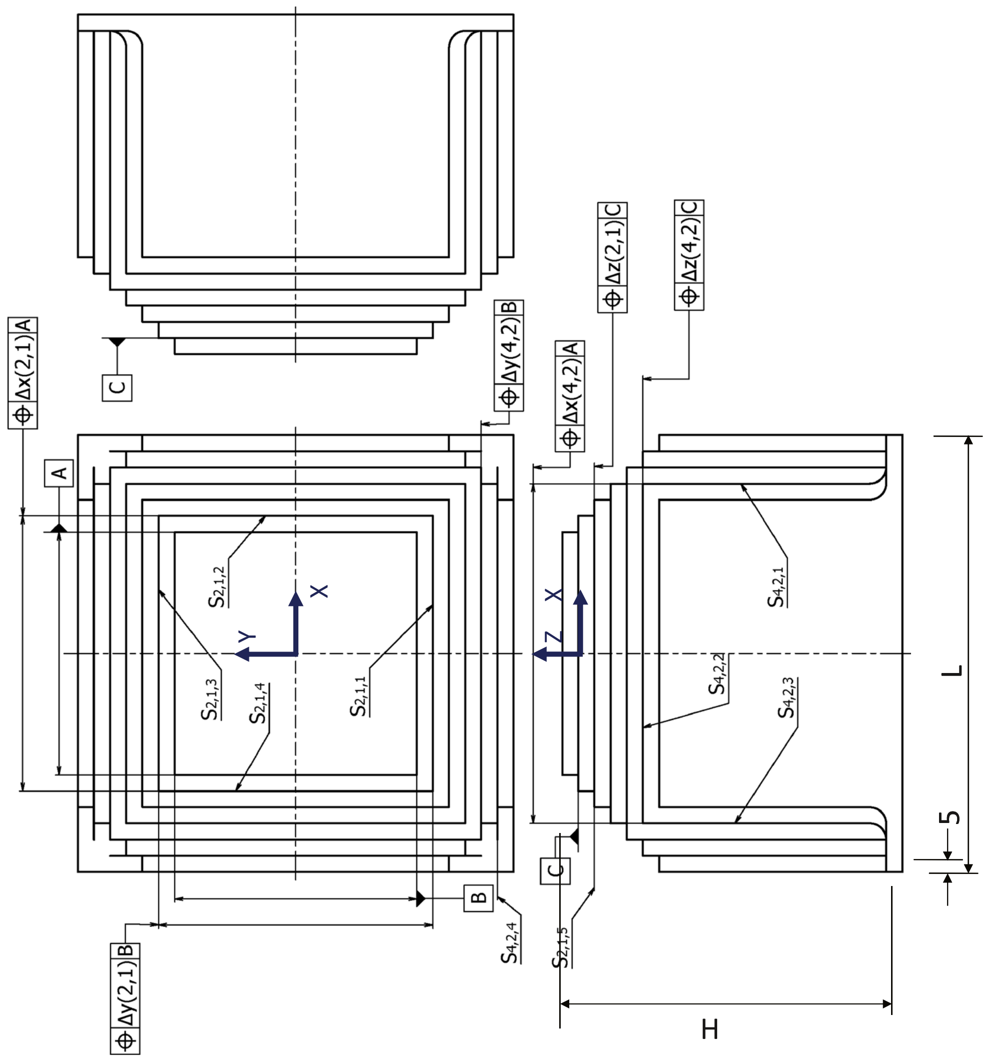

Fig. 3 Nominal geometry of the finished test piece. The geometric tolerance symbols and surface names (S_{**}) are referred in Section 5.3. As examples, geometric errors associated with the step $(i, j) = (2, 1)$ (machined at $c_2 = 90°$ and $b_1 = 0°$) and the step $(i, j) = (4, 2)$ (machined at $c_4 = 270°$ and $b_2 = -90°$) are shown

its derivation can be found in many previous studies, e.g., [27, 28], this subsection only briefly reviews it for the machine configuration in Fig. 1.

Eight location errors in Table 1 represent position and orientation errors of two rotary axis average lines in Fig. 1. As examples, Fig. 5a represents the definition of δz^0_{BT}, and Fig. 5b represents β^0_{RC}. In the viewpoint of kinematic modelling, they represent position and orientation errors of one coordinate system to the other. δz^0_{BT} represents the Z-position error of the B-axis coordinate system to the tool coordinate system (see below. "T" in δz^0_{BT} represents the tool coordinate system). In β^0_{RC}, "R" represents the machine coordinate system. The variation from these "average" positions and orientations is represented by position-dependent geometric errors (error motions) of rotary axis, shown in Table 2.

When C- and B-axes are indexed respectively at c_i and $b_j \in \mathbb{R}$, the TCP position in the machine coordinate system, denoted by ${}^r p(c_i, b_j) \in \mathbb{R}^3$ (the left-hand side superscript ^{r} represents a vector in the machine coordinate system), is formulated with location errors by

$$\begin{bmatrix} {}^r p(c_i, b_j) \\ 1 \end{bmatrix} = {}^r T_t \begin{bmatrix} {}^t p^* \\ 1 \end{bmatrix} \tag{1}$$

$$\begin{aligned} {}^r T_t &= {}^r T_c \cdot {}^c T_b \cdot {}^b T_t \\ {}^b T_t &= D_x(-\delta x^0_{BT}) D_z(-d^*_{BT} - \delta z^0_{BT}) \\ {}^c T_b &= D_x(-\delta x^0_{CB}) D_y(-\delta y^0_{CB}) D_a(-\alpha^0_{CB}) D_b(b_j) \\ {}^r T_c &= D_a(-\alpha^0_{RC}) D_b(-\beta^0_{RC}) D_c(-\gamma^0_{RC}) D_c(c_i) \end{aligned} \tag{2}$$

where ${}^r T_t \in \mathbb{R}^{4\times4}$ represents the homogeneous transformation matrix (HTM) from the tool coordinate system to the machine coordinate system. The tool coordinate system rotates by B- and C-axes and its origin is at the TCP. ${}^t p^* = [0, 0, 0, 1]^T$ represents its origin. ${}^b T_t \in \mathbb{R}^{4\times4}$ represents the HTM from the tool coordinate system to the B-axis coordinate system, i.e., the local coordinate system rotating with B-axis, whose Y-axis is attached to the B-axis

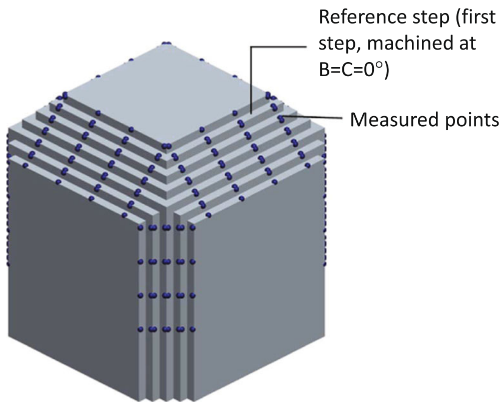

Fig. 4 Measured points on the finished test piece

average line. $D_x(x)$, $D_y(y)$, and $D_z(z) \in \mathbb{R}^{4\times4}$ are the HTM representing the linear translation in the X-, Y-, and Z-directions, respectively. $D_a(a)$, $D_b(b)$, and $D_c(c) \in \mathbb{R}^{4\times4}$ are the HTM representing the rotation about the X-, Y-, and Z-axes, respectively. See, e.g., [27, 28] for their formulation. $d^*_{BT} \in \mathbb{R}$ represents the nominal distance from the B-axis average line to the TCP.

When there is no location error, the command TCP position, ${}^r p^*(c_i, b_j) \in \mathbb{R}^3$ is given by

$$\begin{bmatrix} {}^r p^*(c_i, b_j) \\ 1 \end{bmatrix} = D_c(c_i) D_b(b_j) D_z(-d^*_{BT}) \begin{bmatrix} {}^t p^* \\ 1 \end{bmatrix} \tag{3}$$

Equations (1) and (3) can be rewritten as follows, under the assumption that the location errors are sufficiently small:

$$\begin{aligned} \begin{bmatrix} {}^r p(c_i, b_j) \\ 1 \end{bmatrix} &\approx D_x(\delta x) D_y(\delta y) D_z(\delta z) D_a(\delta a) D_b(\delta b) D_c(\delta c) \begin{bmatrix} {}^r p^*(c_i, b_j) \\ 1 \end{bmatrix} \\ \delta x &= -\left(\delta x^0_{BT} \cos b_j + \delta z^0_{BT} \sin b_j + \delta x^0_{CB}\right) \cos c_i + \delta y^0_{CB} \sin c_i \\ \delta y &= -\left(\delta x^0_{BT} \cos b_j + \delta z^0_{BT} \sin b_j + \delta x^0_{CB}\right) \sin c_i - \delta y^0_{CB} \cos c_i \\ \delta z &= \delta x^0_{BT} \sin b_j - \delta z^0_{BT} \cos b_j \\ \delta a &= -\alpha^0_{CB} \cos c_i - \alpha^0_{RC} \\ \delta b &= -\alpha^0_{CB} \sin c_i - \beta^0_{RC} \\ \delta c &= -\gamma^0_{RC} \end{aligned} \tag{4}$$

Equation (4) indicates that the TCP is displaced by $(\delta x, \delta y, \delta z)$ in X-, Y-, and Z-directions and rotated by $(\delta a, \delta b, \delta c)$ around X-, Y-, and Z-axes by location errors in Table 1. It can be straightforwardly extended to rotary axis position-dependent geometric errors (see [29] for analogous formulation). It is important to note that this paper assumes that linear axis geometric errors are negligibly small relative to those of the rotary axes.

4.2 Identification of rotary axis geometric errors

For each square-shaped step machined at c_i and b_j, denote the kth measured position in the measurement coordinate system by $p(i, j, k) \in \mathbb{R}^3$ ($k = 1, \cdots, N(i, j)$), where $N(i, j) \in \mathbb{R}$ is the number of probed points on the (i, j) step. Suppose that its nominal position is given by $p^*(i, j, k) \in \mathbb{R}^3$.

Denote the displacement of the (i, j) step from its nominal position by $(\Delta x(i, j), \Delta y(i, j), \Delta z(i, j))$ in X-, Y-, and Z-directions. Denote its orientation error by $(\Delta a(i, j), \Delta b(i, j), \Delta c(i, j))$ around X-, Y-, and Z-axes. The first step of the algorithm is to calculate $\Delta x(i, j)$ to $\Delta c(i, j)$ from a set of measured points, $p(i, j, k)$.

They can be calculated by solving the following minimization problem:

$$\min_{\Delta x(i,j), \cdots, \Delta c(i,j)} \sum_k \left\{\Delta p(i, j, k) \cdot n^*(i, j, k)\right\}^2 \tag{5}$$

Table 1 Position and orientation errors of rotary axis average lines (location errors)

Symbol	Description
δx^0_{BT}	Position error of B-axis average line to TCP in X-direction
δz^0_{BT}	Position error of B-axis average line to TCP in Z-direction
δx^0_{CB}	Position error of C- to B-axis average line in X-direction
δy^0_{CB}	Position error of C- to B-axis average line in Y-direction
α^0_{CB}	Squareness error of B- to C-axes
α^0_{RC}	Squareness error of Y- to C-axes
β^0_{RC}	Squareness error of X- to C-axes
γ^0_{RC}	Squareness error of B- to X-axes at $C = 0°$

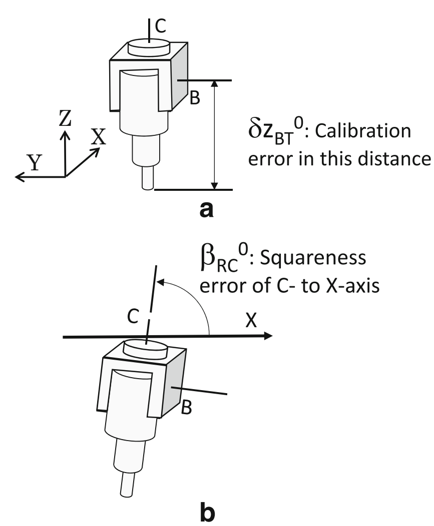

Fig. 5 Definition of location errors. **a** δz^0_{BT}. **b** β^0_{RC}

where $n^*(i,j,k) \in \mathbb{R}^3$ is a unit vector representing the normal direction to the target surface, and

$$\begin{aligned}\Delta p(i,j,k) &= p(i,j,k) - \hat{p}(i,j,k)\\ \begin{bmatrix}\hat{p}(i,j,k)\\ 1\end{bmatrix} &= D_x(\Delta x(i,j))D_y(\Delta y(i,j))D_z(\Delta z(i,j))\\ &\qquad D_a(\Delta a(i,j))D_b(\Delta b(i,j))D_c(\Delta c(i,j))\begin{bmatrix}p^*(i,j,k)\\ 1\end{bmatrix}\end{aligned} \tag{6}$$

$(\Delta x(i,j), \Delta y(i,j), \Delta z(i,j))$ represents the position error of the TCP trajectory (a square path) in the machine coordinate system. Therefore, $(\Delta x(i,j), \Delta y(i,j), \Delta z(i,j))$ should be equal to ${}^r p(c_i, b_j) - {}^r p^*(c_i, b_j)$ in Eqs. (4) and (3). Note that the tool's orientation error, represented by $(\delta a, \delta b, \delta c)$ in Eq. (4), does not influence the orientation of each square step, $(\Delta a(i,j), \Delta b(i,j), \Delta c(i,j))$.

Each step's position, $\Delta x(i,j)$ to $\Delta z(i,j)$, is measured in reference to the reference step, machined at $b_1 = c_1 = 0°$. The influence of rotary axis location errors to the measurement coordinate system must be taken into consideration. Therefore, rotary axis location errors (Table 1) can be obtained by solving

$$\min_{\delta x^0_{BT},\cdots,\gamma^0_{RC}} \sum_{i,j} \left\| \left\{ \left({}^r p(c_i,b_j) - {}^r p^*(c_i,b_j)\right) - \left({}^r p(0,0) - {}^r p^*(0,0)\right) \right\} - \begin{bmatrix}\Delta x(i,j)\\ \Delta y(i,j)\\ \Delta z(i,j)\end{bmatrix} \right\|_2 \tag{7}$$

where ${}^r p(c_i, b_j)$ and ${}^r p^*(c_i, b_j)$ are respectively given in Eqs. (4) and (3) and $\Delta x(i,j)$ to $\Delta z(i,j)$ are calculated by Eq. (5). The C-axis position-dependent geometric errors in Table 2 can be analogously identified by extending this formulation (see [29] for analogous formulation).

Remark When the tool length is constant, the influence of radial and axial error motions of B- and C-axes on the TCP position cannot be distinguished from that of their tilt and angular positioning error motions. To separate them, the machining test should be repeated with different tool lengths. This paper does not consider B- and C-axis tilt and angular positioning error motions.

5 Case study

5.1 Test setup

The machine configuration is shown in Fig. 1. The machine's major specifications are shown in Table 3. Table 4 shows the machining conditions. The machining conditions (feed per tooth, radial depth of cut, cutting speed, and cutting direction) were chosen from typical finishing conditions for this workpiece, tool, and machine, such that the finished surface roughness becomes sufficiently small compared to the finished test piece's geometric error. The nominal radial depth of cut was zero (i.e., the "zero cut," where the same surface is nominally cut after the semi-finishing with the radial depth of cut, 0.1 mm) such that the influence of tool deflection due to the cutting force is minimized. Before the machining test, the machine was sufficiently warmed up with continuous spindle rotation. The finished test piece's nominal geometry was $L = H = 135$ mm in Fig. 3. Only a single test piece was finished in this experiment.

5.2 Graphical presentation of the finished test piece's geometry

Figure 6 shows the geometry of the finished test piece measured by a CMM. The difference between the nominal probed point (red dot) and the measured point (green dot) is magnified 50 times in the direction normal to the surface. In other words, when the measured point is displaced by 400 μm from its command position, this difference is shown as 20 mm in Fig. 6 (see "Error scale"). The gray-painted polygon represents the mean surface calculated by using the least square fit to the measured points.

Table 2 Position-dependent geometric errors (error motions) of C-axis

Symbol	Description
$\delta x_{RC}(c_i)$	Radial error motion of C-axis in X-direction
$\delta y_{RC}(c_i)$	Radial error motion of C-axis in Y-direction
$\delta z_{RC}(c_i)$	Axial error motion of C-axis in Z-direction
$\alpha_{RC}(c_i)$	Tilt error motion of C-axis around X-axis
$\beta_{RC}(c_i)$	Tilt error motion of C-axis around Y-axis
$\gamma_{RC}(c_i)$	Angular positioning error motion of C-axis

Table 3 Major specification of machine tool

Stroke	X, 4065 mm; Y, 3500 mm; Z, 1016 mm
	C, ± 360°; B, ± 110°
Drive	X, Y, Z: ball screw and servo motor
	C, B: direct drive
Guideway	Y, Z: slide guideway
	C, B: axial-radial cylindrical roller bearing

Table 4 Major machining conditions

Tool	Tungsten carbide radius end mill, $\phi 8$ mm, 3 flutes
Workpiece material	Aluminum alloy JIS A5061
Feed per tooth	0.075 mm/tooth
Axial depth of cut	5 mm
Radial depth of cut	0 mm (zero cut)
Cutting speed	600 m/min
Milling direction	Down cut

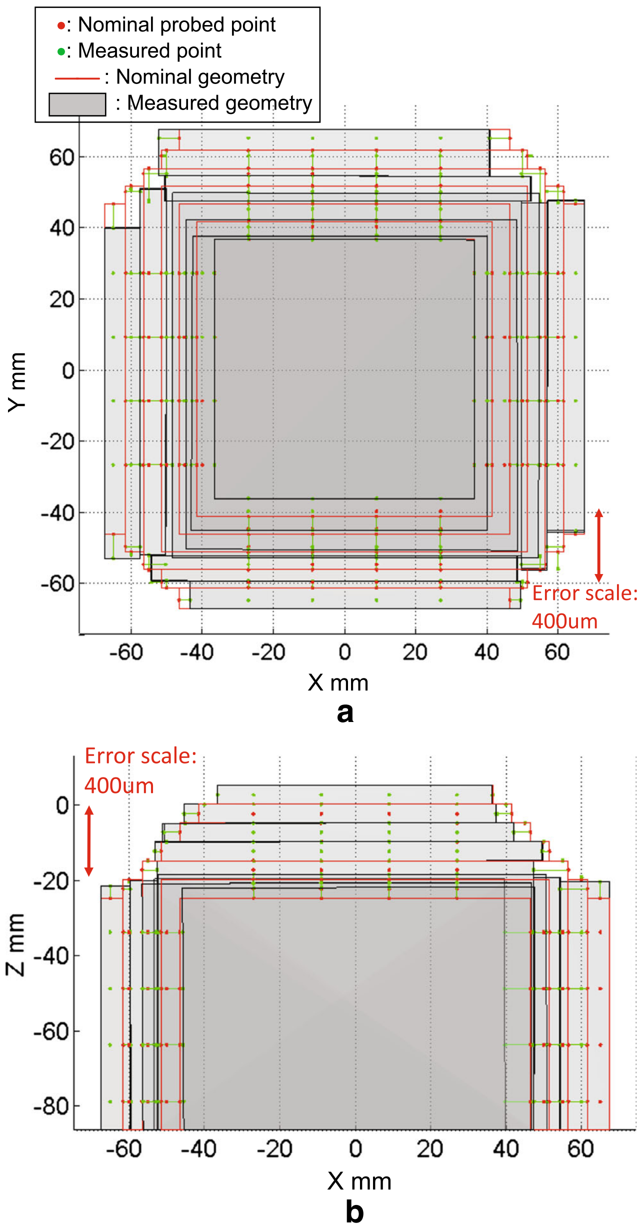

Fig. 6 The finished test piece's geometry measured by using a CMM. The error from the nominal point to the measured point is magnified 50 times. The gray-painted polygon represents the mean surface calculated from the measured points. **a** Projection onto the *XY* plane and **b** projection onto the *XZ* plane

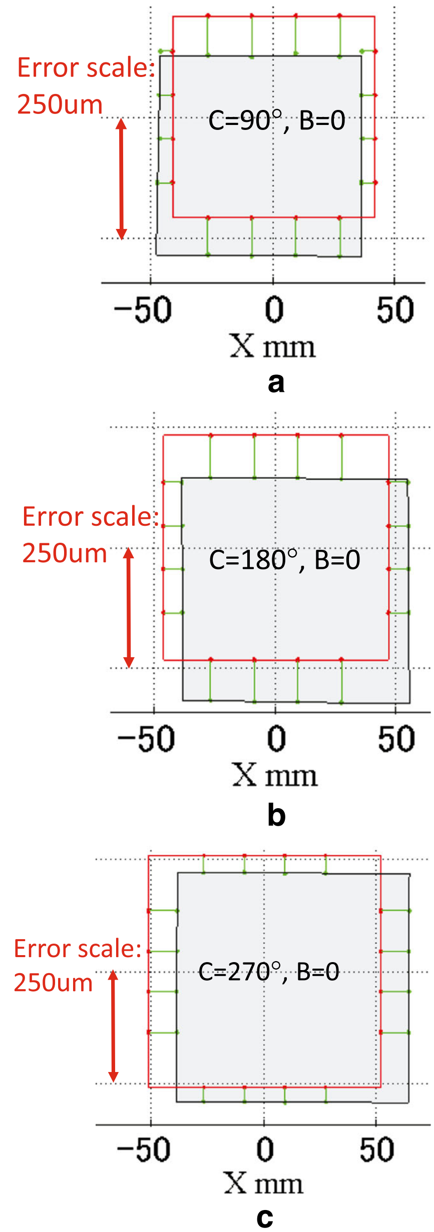

Fig. 7 The second, third, and fourth steps in Fig. 6 (projected onto the *XY* plane). **a** The second step, $(i, j) = (2, 1)$, machined at $c_i = 90°, b_j = 0°$, **b** the third step, $(i, j) = (3, 1)$, machined at $c_i = 180°, b_j = 0°$, and **c** the fourth step, $(i, j) = (4, 1)$, machined at $c_i = 270°, b_j = 0°$

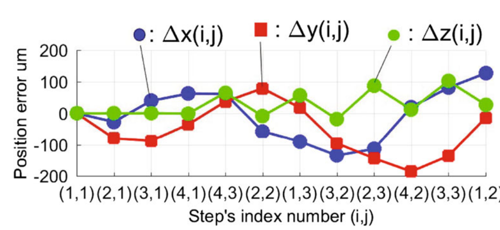

Fig. 8 Position errors, $\Delta x(i, j)$ to $\Delta z(i, j)$, of each step measured by a CMM. Step's index numbers correspond to *C*- and *B*-axis angular positions, $c_i = 0, 90, 180, 270°$ $(i = 1, 2, 3, 4)$ and $b_j = 0, -90, 90°$ $(j = 1, 2, 3)$

Table 5 Description of $\Delta x(i, j)$ to $\Delta z(i, j)$ defined in Section 4.2, according to the GD&T definition

a)	
$\Delta x(2, 1)$	Position error in X-direction of the mean plane of $S_{2,1,2}$ and $S_{2,1,4}$ in reference to the datum surface A
$\Delta y(2, 1)$	Position error in Y-direction of the mean plane of $S_{2,1,1}$ and $S_{2,1,3}$ in reference to the datum surface B
$\Delta z(2, 1)$	Position error in Z-direction of the surface $S_{2,1,5}$ in reference to the datum surface C
b)	
$\Delta x(4, 2)$	Position error in X-direction of the mean plane of $S_{4,2,1}$ and $S_{4,2,3}$ in reference to the datum surface A
$\Delta y(4, 2)$	Position error in Y-direction of the surface $S_{4,2,4}$ in reference to the datum surface B
$\Delta z(4, 2)$	Position error in Y-direction of the surface $S_{4,2,2}$ in reference to the datum surface C

See also Fig. 3. a) Position errors of the step, $(i, j) = (2, 1)$, machined at $c_2 = 90°$ and $b_1 = 0°$. The errors of three steps on the top face, $i = 1, 2, 3$ and $j = 1$, are defined analogously. b) Position errors of the step, $(i, j) = (4, 2)$, machined at $c_4 = 270°$ and $b_2 = -90°$. The errors of eight steps on side faces, $i = 1, \cdots, 4$ and $j = 2, 3$, are defined analogously

For clearer presentation, Fig. 7 shows the projection onto the XZ plane of (a) the second step, $(i, j) = (2, 1)$, machined at $c_i = 90°, b_j = 0°$, (b) the third step, $(i, j) = (3, 1)$, machined at $c_i = 180°, b_j = 0°$, and (c) the fourth step, $(i, j) = (4, 1)$, machined at $c_i = 270°, b_j = 0°$. It can be clearly observed that these steps are displaced to X- and Y-directions by about 100 μm at maximum.

5.3 Geometric errors of the finished test piece

The position errors of each step, $\Delta x(i, j)$ to $\Delta z(i, j)$, calculated by solving (5), are shown in Fig. 8. The first step, machined at $c_1 = b_1 = 0°$, is the reference step and thus does not have any error. For example, the second step, $(i, j) = (2, 1)$, has the position error in the X-direction by about − 20 μm to the datum surface A (see Fig. 3) and in the Y-direction by about − 70 μm to the datum surface B. This position error can be also observed in Fig. 7a.

$\Delta x(i, j)$ to $\Delta z(i, j)$ can be interpreted as the geometric dimensioning and tolerancing (GD&T) geometric errors [30]. Figure 3 shows the GD&T symbols (only the geometric errors for the steps $(i, j) = (2, 1)$ (Table 5a) and $(i, j) = (4, 2)$ (Table 5b) are shown as examples). Their correspondence to $\Delta x(i, j)$ to $\Delta z(i, j)$ are shown in Table 5.

With good understanding of the five-axis kinematics presented in Section 4.1, a user can intuitively observe the machine's error motions from Figs. 6 and 8. For example, X- and Y-position errors of three steps, $(i, j) = (2, 1)$ to $(4, 1)$, shown in Fig. 7, are mostly caused by the position error of the C- to the B-axis average line (Δx^0_{CB} and Δy^0_{CB}), as well as the position error of the B-axis average line with respect to the tool tip (Δx^0_{BT}).

5.4 Numerical parameterization of rotary axis geometric errors

From measured geometric errors of the finished test piece, position and orientation errors of rotary axis average lines (location errors) were identified by using the algorithm presented in Section 4.2. The estimates are shown in Table 6a) ("By machining test (without compensation)"). Similarly, position-dependent geometric errors of C-axis are identified as shown in Fig. 9. It is to be noted that angular errors in Table 6 are not significant compared to possible uncertainty

Table 6 Position and orientation errors of rotary axis average lines (location errors) identified from a) the finished test piece's geometry without the compensation, b) the R-test, and c) the finished test piece's geometry with the compensation

Symbol	a) By machining test (without compensation)	b) By R-test (without compensation)	c) By machining test (with compensation)
δx^0_{BT}	38.1 μm	31.4 μm	2.7 μm
δz^0_{BT}	75.1 μm	49.4 μm	16.3 μm
δx^0_{CB}	−21.2 μm	−21.6 μm	1.6 μm
δy^0_{CB}	−61.0 μm	−59.8 μm	0.5 μm
α^0_{BC}	0.9 mdeg	0.7 mdeg	0.2 mdeg
α^0_{RC}	0.2 mdeg	0.5 mdeg	−0.2 mdeg
β^0_{RC}	2.9 mdeg	2.8 mdeg	−0.3 mdeg
γ^0_{RC}	2.2 mdeg	0.5 mdeg	2.3 mdeg

See Table 1 for their definition

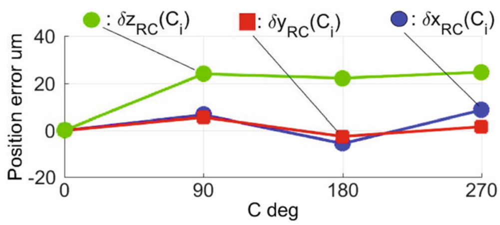

Fig. 9 Identified position-dependent geometric errors of *C*-axis. See Table 2 for their definition

contributors. For example, $\gamma_{RC}^0 = 2.2$ mdeg displaces the steps machined at $b_j = -90$ or 90° by 6.5 μm, since the distance to the tool tip to the *B*-axis of rotation is $d_{BT}^* = 170.2$ mm. This influence is significantly smaller than actual position errors of each step, $\Delta x(i, j)$ to $\Delta z(i, j)$, shown in Fig. 8. This could partly cause relatively larger difference in the estimates of γ_{RC}^0 by the machining test and the R-test.

5.5 Error compensation by R-test

As was reviewed in Section 1, many "indirect" tests are available to identify position and orientation errors of rotary axis average lines. The R-test is one of them. The R-test was first presented by Weikert [31]. Its application to the identification of rotary axis location errors was presented by Knapp and Bringmann [32] and its extension to position-dependent geometric errors was presented in [29]. It can be applied to the tests in ISO 10791-6:2014 [6]. A part of the authors developed software [33], now commercially available from Fukuda Corp. ("http://www.fukudaco.co.jp/"), to perform and analyze the R-test. Based on the estimates by the R-test, the software can generate a compensation table to cancel the influence of rotary axis location errors and position-dependent geometric errors. This subsection presents an experimental demonstration of the

Fig. 10 The R-test measuring instrument

present pyramid-shaped machining test to investigate the effectiveness of such a numerical compensation. The R-test instrument, its measurement procedure, its analysis methodology, and the numerical compensation are described in details in past publications [29, 31–33] and, thus, are not repeated here.

Figure 10 shows (a) the R-test instrument and (b) its installment on the machine shown in Fig. 1. The R-test results were reported in our previous publication [33]. Table 6b) shows rotary axis location errors identified by the R-test.

The pyramid-shaped machining test was performed under the numerical compensation of location errors and *C*-axis position-dependent geometric errors, identified by the

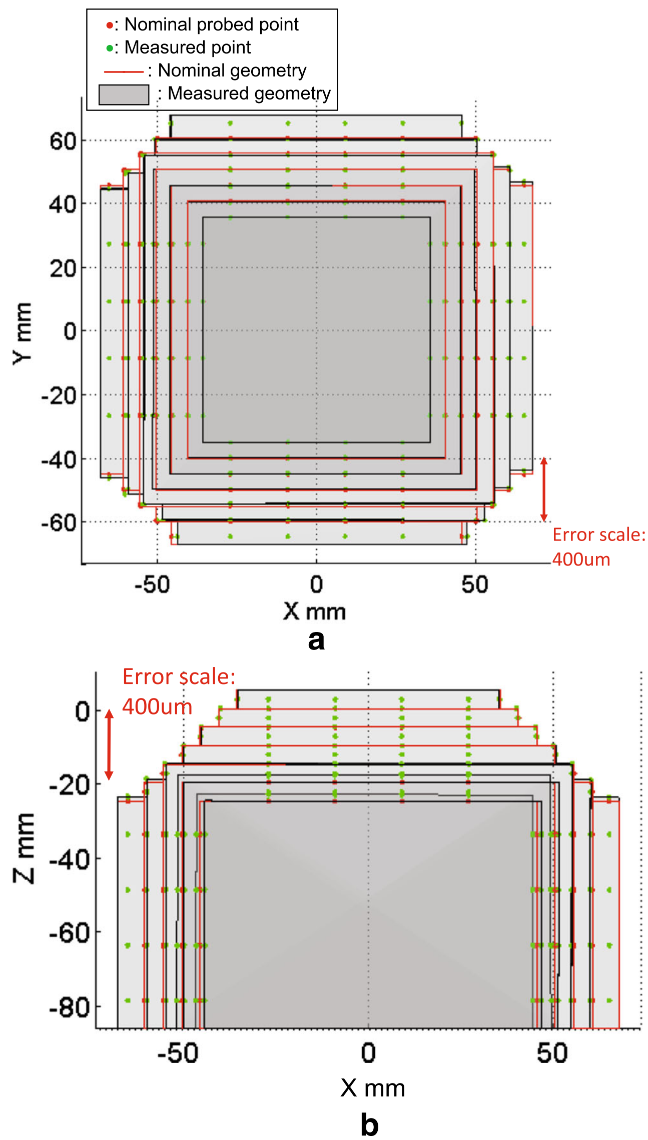

Fig. 11 The finished test piece's geometry under the numerical compensation of rotary axis position-dependent geometric errors identified by the R-test. **a** Projection onto the *XY* plane and **b** projection onto the *XZ* plane

R-test. The "3D rotary error compensation" function in some Fanuc controllers [35] was used. Similar compensation is possible on many latest CNC systems, e.g., Siemens and Heidenhain controllers. Figure 11 shows the geometry of the machined test piece under this compensation. Figure 12 shows the position errors of each step, $\Delta x(i, j)$ to $\Delta z(i, j)$. Comparing Fig. 11 with Fig. 6 (and Fig. 12 with Fig. 8), it can be clearly observed that the test piece's geometric error was significantly reduced. Table 6c) shows rotary axis location errors identified from the finished test piece.

5.6 Discussion

Considering the uncertainty caused by the machine's repeatability error or the machining process, Table 6c) shows that most location errors were reduced to a sufficiently small value. For example, without the compensation, the position error of the C-axis average line was $(\delta x^0_{CB}, \delta y^0_{CB}) = (-21.2, -61.0)$ μm. By applying the numerical compensation, it was reduced to $(\delta x^0_{CB}, \delta y^0_{CB}) = (1.6, 0.5)$ μm.

In Table 6c), the position error of B-axis average line in the Z-direction, δz^0_{BT}, is relatively larger, even after the compensation. This is likely caused by the thermal expansion of the spindle unit. The R-test was performed when the spindle was stopped. When the machining test was performed, the rotating spindle generates the heat and displaces the TCP to the Z-direction. The present machining test can evaluate rotary axis geometric errors under the thermal influence of the spindle rotation. This is one of advantages of a machining test over non-cutting tests. By repeating this test periodically, the thermal deformation of the machine structure may be observed. The thermal deformation tests in ISO 230-3 [36] do not involve any machining operations. Such an application of the machining test will be studied in future.

A potential issue for the present machining test is the influence of linear axis error motions. The algorithm presented in Section 4.2 ignores linear axis error motions, and thus, they can be a potential uncertainty contributor for the estimated rotary axis geometric errors. This influence was discussed in the uncertainty analysis presented in our previous work [20].

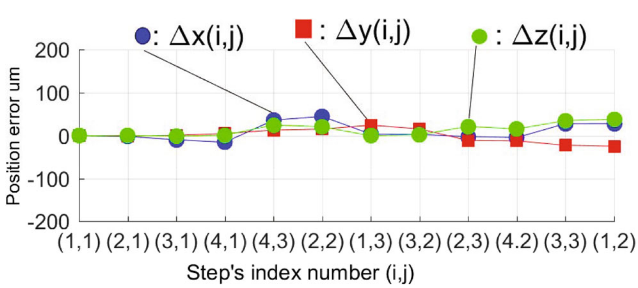

Fig. 12 Position errors, $\Delta x(i, j)$ to $\Delta z(i, j)$, of each step under the numerical compensation in Fig. 11. Step's index numbers correspond to C- and B-axis angular positions, $c_i = 0, 90, 180, 270°$ ($i = 1, 2, 3, 4$) and $b_j = 0, -90, 90°$ ($j = 1, 2, 3$)

6 Conclusion

The software was developed to perform and analyze the pyramid-shaped machining test proposed in our previous work [20]. As this paper's original contribution, the extension of the analysis algorithm in [20] to a five-axis machine tool with two rotary axes on the tool side was presented. An experimental case study was presented to illustrate the functionalities of the developed software. The experiment showed that position and orientation errors (location errors) of rotary axis average lines, as well as position-dependent error motions of a rotary axis, can be identified from geometric errors of the finished test piece. Experimental demonstration of the numerical compensation of rotary axis geometric errors based on the R-test, along with its performance investigation by applying the present machining test, was also this paper's original contribution. The geometric error of the finished test piece showed that there was the position error of the C-axis average line, $(\delta x^0_{CB}, \delta y^0_{CB}) = (-21.2, -61.0)$ μm. By applying the numerical compensation, it was reduced to $(\delta x^0_{CB}, \delta y^0_{CB}) = (1.6, 0.5)$ μm, which was verified by the present machining test.

The developed software is commercially available from Fukuda Corporation as "FKD Machining Test Analyzer System" ("http://www.fukudaco.co.jp/"). Currently, the software supports five-axis machines with (1) a universal head (two rotary axes on the spindle side) (the analysis algorithm is presented in this paper), (2) a tilting rotary table (two rotary axes on the work table side) (the algorithm was presented in [20]), and (3) one rotary axis on the spindle side, and one rotary axis on the table side (including a mill-turn center with a swivel head) (the algorithm is essentially the combination of (1) and (2)).

Acknowledgments This work was supported by JSPS KAKENHI Grant Number JP15K05721.

References

1. ISO 230-1:2012, Test code for machine tools—part 1: geometric accuracy of machines operating under no-load or quasi-static conditions, 2012
2. ISO 230-7:2006, Test code for machine tools—part 7: geometric accuracy of axes of rotation
3. Schwenke H, Knapp W, Haitjema H, Weckenmann A, Schmitt R, Delbressine F (2008) Geometric error measurement and compensation of machines—an update. CIRP Ann - Manuf Technol 57(2):560–575

4. Ibaraki S, Knapp W (2012) Indirect measurement of volumetric accuracy for three-axis and five-axis machine tools: a review. Int J Autom Technol 6(2):110–124
5. ISO 10791-1:2015, Test conditions for machining centres—part 1: geometric tests for machines with horizontal spindle (horizontal Z-axis)
6. ISO 10791-6:2014, Test conditions for machining centers—part 6: accuracy of speeds and interpolations
7. ISO 10791-7:2015, Test conditions for machining centres—part 7: accuracy of a finished test piece
8. NAS979:1969, Uniform cutting test—NAS series, metal cutting equipment specifications, 34-37
9. Bossoni S, Cupic J (2007) Test piece for simultaneous 5-axis machining. In: Laser metrology and machine performance VIII, Proceedings of 8th international conference on laser metrology, pp 24–33
10. Hong C, Ibaraki S, Matsubara A (2011) Influence of position-dependent geometric errors of rotary axes on a machining test of cone frustum by five-axis machine tools. Precis Eng 35(1):1–11
11. Jiang Z, Ding J, Song Z (2015) Modeling and simulation of surface morphology abnormality of ‘S’ test piece machined by five-axis CNC machine tool. Int J Adv Manuf Technol 1–15
12. Wang W, Jiang Z, Tao W (2015) A new test part to identify performance of five-axis machine tool—part I: geometrical and kinematic characteristics of S part. Int J Adv Manuf Technol 79:1–10
13. ISO 10791-7:2014/DAmd, Test conditions for machining centres—part 7: accuracy of finished test pieces, Amendment 1, Annex A: Accuracy of a finished free form test piece
14. Ohta K, Li Z, Tsutsumi M (2012) Proposal of a machining test of five-axis machining centers using a truncated square pyramid. Key Eng Mater 523-524:475–480
15. Takeshima H, Ihara Y (2009) Finished test piece example for five-axis machining centers. In: Proceedings international conference on leading edge manufacturing in 21st century, pp 123–126
16. Hasegawa S, Sato R, Shirase K (2016) Influences of geometric and dynamic synchronous errors onto machined surface in 5-axis machining center. J Adv Mech Des, Syst, Manuf 10(5):JAMDSM0071
17. Lin P, Tzeng C (2008) Modeling and measurement of active parameters and workpiece home position of a multi-axis machine tool. Int J Mach Tools Manuf 48-3/4:338–349
18. Bono M, Kroll J (2008) Tool setting on a B-axis rotary table of a precision lathe. Int’l J Mach Tools Manuf 48(11):1261–1267
19. Yamamoto T, Hasebe T, Tsutsumi M (2011) Development of testing method for five-axis machining centers by thin groove cutting. J Jpn Soc Precis Eng 77(4):405–409. (in Japanese)
20. Ibaraki S, Ota Y (2014) A machining test to calibrate rotary axis error motions of five-axis machine tools and its application to thermal deformation test. Int J Mach Tools Manuf 86:81–88
21. Velenosi A, Campatelli G, Scippa A (2015) Axis geometrical errors analysis through a performance test to evaluate kinematic error in a five axis tilting-rotary table machine tool. Precis Eng 39:224–233
22. Wojciechowski S, Chwalczuk T, Twardowski P, Krolczyk GM (2015) Modeling of cutter displacements during ball end milling of inclined surfaces. Arch Civ Mech Eng 15(4):798–805
23. Wojciechowski S, Twardowski P, Pelic M, Maruda RW, Barrans S, Krolczyk GM (2016) Precision surface characterization for finish cylindrical milling with dynamic tool displacements model. Precis Eng 46:158–165
24. Wojciechowski S, Maruda RW, Nieslony P, Krolczyk GM (2016) Investigation on the edge forces in ball end milling of hardened steel. Int J Mech Sci 119:360–369
25. Lazoglu I, Boz Y, Erdim H (2011) Five-axis milling mechanics for complex free form surfaces. Ann CIRP – Manuf Technol 60: 117–20
26. Iwabe H, Kikuchi K, Futakawa M, Kazama Y (2015) Study on cutting mechanism and cutting performance of inclined surface machining with radius end mill—comparison with cutting method of contouring path and scanning path –. J Jpn Soc Precis Eng 81(7):655–660
27. Abbaszaheh-Mir Y, Mayer JRR, Clotier G, Fortin C (2002) Theory and simulation for the identification of the link geometric errors for a five-axis machine tool using a telescoping magnetic ball-bar. Int J Prod Res 40(18):4781–4797
28. Inasaki I, Kishinami K, Sakamoto S, Sugimura N, Takeuchi Y, Tanaka F (1997) Shaper generation theory of machine tools—its basis and applications. Yokendo, Tokyo. (in Japanese)
29. Ibaraki S, Oyama C, Otsubo H (2011) Construction of an error map of rotary axes on a five-axis machining center by static R-test. Int J Mach Tools Manuf 51:190–200
30. ISO 1101:2017, Geometrical product specifications (GPS)—geometrical tolerancing—tolerances of form, orientation, location and run-out
31. Weikert S (2004) R-test; a new device for accuracy measurements on five axis machine tools. CIRP Ann - Manuf Technol 53(1): 429–432
32. Knapp W, Bringmann B (2006) Model-based ’Chase-the-Ball’ calibration of a 5-axis machining center. CIRP Ann - Manuf Technol 55(1):531–534
33. Ibaraki S, Nagai Y, Otsubo H, Sakai Y, Morimoto S, Miyazaki Y (2015) R-test analysis software for error calibration of five-axis machine tools—application to a five-axis machine tool with two rotary axes on the tool side–. Int J Autom Technol 9(4):387–395
34. Hong C, Ibaraki S (2012) Graphical presentation of error motions of rotary axes on a five-axis machine tool by static R-test with separating the influence of squareness errors of linear axes. Int J Mach Tools Manuf 59:24–33
35. Yamada Y (2012) Compensation technology for volumetric error in machine tool. In: Proceedings of the 15th international machine tool engineers’ conference
36. ISO 230-3:2007, Test code for machine tools—part 3: determination of thermal effects